



UNIVERSITY OF LEEDS

This is a repository copy of *Seawater operating bio-photovoltaic cells coupling semiconductor photoanodes and enzymatic biocathodes*.

White Rose Research Online URL for this paper:  
<http://eprints.whiterose.ac.uk/131235/>

Version: Accepted Version

---

**Article:**

Zhang, L, Álvarez-Martos, I, Vakurov, A et al. (1 more author) (2017) Seawater operating bio-photovoltaic cells coupling semiconductor photoanodes and enzymatic biocathodes. *Sustainable Energy and Fuels*, 1 (4). pp. 842-850. ISSN 2398-4902

<https://doi.org/10.1039/C7SE00051K>

---

© 2017 The Royal Society of Chemistry. This is an author produced version of a paper published in *Sustainable Energy and Fuels*. Uploaded in accordance with the publisher's self-archiving policy.

**Reuse**

Items deposited in White Rose Research Online are protected by copyright, with all rights reserved unless indicated otherwise. They may be downloaded and/or printed for private study, or other acts as permitted by national copyright laws. The publisher or other rights holders may allow further reproduction and re-use of the full text version. This is indicated by the licence information on the White Rose Research Online record for the item.

**Takedown**

If you consider content in White Rose Research Online to be in breach of UK law, please notify us by emailing [eprints@whiterose.ac.uk](mailto:eprints@whiterose.ac.uk) including the URL of the record and the reason for the withdrawal request.



[eprints@whiterose.ac.uk](mailto:eprints@whiterose.ac.uk)  
<https://eprints.whiterose.ac.uk/>



## Seawater Operating Bio-Photovoltaic Cells Coupling Semiconductor Photoanodes and Enzymatic Biocathodes

Lingling Zhang,<sup>a</sup> Isabel Álvarez-Martos,<sup>a</sup> Alexander Vakurov,<sup>a</sup> and Elena E. Ferapontova<sup>\*a</sup>

Received 00th January 20xx,  
Accepted 00th January 20xx

DOI: 10.1039/x0xx00000x

www.rsc.org/

Access to fresh water and energy is ranked as one of the most severe challenges to humankind. Restricted availability of fossil fuels and clean water does not match the increasing energy demands and growing population needs, which, desirably, should be satisfied in the most sustainable, clean and inexpensive way. Here, we report clean and sustainable conversion of solar energy into electricity by photo- and bio-electrocatalytic recycling of the H<sub>2</sub>O/O<sub>2</sub> redox couple in a hybrid bio-photovoltaic (BPV) membraneless cell comprising a sunlight-illuminated water-oxidizing semiconductor anode (either Zn-doped hematite or TiO<sub>2</sub>) and an oxygen-reducing enzymatic biocathode, in such environmental media as seawater. Upon simulated solar light illumination (AM 1.5G, 100 mW cm<sup>-2</sup>), the maximum power density ( $P_{\max}$ ) generated by the cell was 236 and 21.4  $\mu\text{W cm}^{-2}$  in 1 M Tris-HCl and seawater, both pH 8, correspondingly. In seawater its ionic content inhibited mostly the activity of the photoanode, but not of the biocathode. The obtained  $P_{\max}$  values were orders of magnitude higher than those of a photo-electrochemical cell with a Pt mesh cathode (0.32  $\mu\text{W cm}^{-2}$  in seawater). Demonstrated thermodynamically feasible coupling of cost-effective photoactive materials such as TiO<sub>2</sub> or hematite semiconductors and enzymatic counterparts in seawater media opens a perspective clean and sustainable way of transformation of the most abundant, clean and renewable source of energy - solar light - and the most massive Earth's water resource - seawater - into electricity, which can also be used for a fresh water production.

### Introduction

Accessibility of fresh water and sustainable energy to everyone is ranked as one of the most severe challenges to humankind, and there is an industrial need for smarter solutions leading to sustainable production of energy and its use for production of fresh water for domestic use. In particular, sustainable development of the society requires alleviation of non-renewable resources such as fossil fuels and their replacement by sustainable and inexpensive sources of energy<sup>1, 2</sup>. Among those, solar energy is considered as the most abundant renewable resource available on the Earth; however, its utilization efficiency has not yet exceeded 1% of the total energy amount landing on the Earth's surface.<sup>3-5</sup> During last decades, a remarkable improvement has been achieved in conversion of solar energy into electricity by photovoltaic solar cells<sup>6-8</sup>, and currently over 80% of the solar market is dominated, not the least due to the well-developed silicon industry, by the crystalline silicon-based solar cell technology able to convert full sunlight into electricity with efficiency of 25% (with an absolute theoretical limit of 32%<sup>9</sup>)<sup>10, 11</sup>. However, a quite high expenditure and relatively low incident

photon-to-electron conversion efficiency of silicon solar cells do not allow to fully satisfy constantly increasing energy demands<sup>12</sup> and trigger the search for more efficient and lower-cost solar cell technologies<sup>13</sup>. Insufficient sustainability of silicon cell production and the necessity of solar cell panel recycling/scraping becomes another vital reason for looking for new solutions<sup>14</sup>.

Dye-sensitized solar cells<sup>15</sup>, polymer solar cells<sup>16, 17</sup> and perovskite solar cells<sup>18, 19</sup> that rely on more abundant semiconductor nanomaterials seem to provide some cost-effective solutions for utilization of solar energy. For example, in the dye-sensitized solar cells, inexpensive titania nanoparticles offer certain advantages over more expensive silicon. Along with that, the incident light conversion efficiency restricted by 12.3-14.1%, discussed stability issues of dye components<sup>20</sup>, and relatively high market prices<sup>21</sup> interfere with their wider applications.

Among sustainable solutions, biological photosystems wired to electrodes for bioelectrocatalytic water oxidation have been explored<sup>22-25</sup>. Such systems are of huge fundamental interest, but practically they are quite expensive, complex in preparation, often insufficiently stable and low-efficient, and thus have low perspectives of commercialization.

In this context, one of the attractive solar energy transformation solutions are photoelectrochemical (PEC) cells that harvest solar energy for electrochemical splitting of water into molecular oxygen and hydrogen that can be further used as a fuel; with that, solar energy is transformed and stored in the

<sup>a</sup> Interdisciplinary Nanoscience Center (iNANO), Science and Technology, Aarhus University, Gustav Wieds Vej 1590-14, DK-8000 Aarhus C, Denmark.  
E-mail: [elena.ferapontova@inano.au.dk](mailto:elena.ferapontova@inano.au.dk); Tel: +45-87156703.

† Electronic Supplementary Information (ESI) available. See DOI: 10.1039/x0xx00000x

form of chemical bonds.<sup>26</sup> Such artificial photosynthesis devices pioneered in early 70<sup>th</sup><sup>27</sup> can be routinely used for production of H<sub>2</sub> fuel (e.g. at a Pt cathode) by oxidation of water to O<sub>2</sub> and H<sup>+</sup> at a sunlight-illuminated semiconductor anode at potentials far less positive than the standard potential of electrochemical water decomposition (1.23 V) or H<sub>2</sub> evolution.

Photo-driven electrooxidation of water can be catalysed by a variety of n-type metal oxide semiconductor materials<sup>28-32</sup>, and TiO<sub>2</sub>, Fe<sub>2</sub>O<sub>3</sub> nanomaterials and/or their nanocomposites may be considered as cost-effective alternative to biological photocatalysts<sup>28-31</sup>. Due to the one of the most negative potentials for water splitting and low cost, TiO<sub>2</sub> represents one of the most perspective photoanode materials for PEC applications<sup>8, 33</sup>, while hematite ( $\alpha$ -Fe<sub>2</sub>O<sub>3</sub>), not so competitive in sense of water oxidation potentials, has its own advantages, such as favourable light absorption ability with a band gap of 1.9-2.2 eV, excellent mechanical stability and chemical inertness in neutral and alkaline environments<sup>34, 35</sup>. A significant improvement of the photo-electrocatalytic activity of hematite photoanodes has been achieved during last years, e.g. hematite's inherent high electron-hole recombination rate had been overcome by material nanostructuring, doping and surface passivation<sup>36-41</sup>.

Hitherto, artificial photosynthesis devices have been considered mostly for the production of H<sub>2</sub> fuel<sup>7, 8</sup>. Here, we explore an alternative, low-cost and sustainable way for photoelectrochemical transformation of solar energy into electricity (that can also be used for fresh water production) in the Earth's most available electrolyte, seawater. For this, we coupled photoelectrocatalytic oxidation of H<sub>2</sub>O to O<sub>2</sub> at a semiconductor anode<sup>42</sup> and O<sub>2</sub> reduction to water at a biocathode comprising an O<sub>2</sub> reducing enzyme immobilized on an inexpensive carbon-cloth cathode<sup>43</sup> (Figure 1). Potentials for photoelectrocatalytic oxidation of water at both titania electrodes<sup>33</sup> and Zn-doped hematite<sup>38</sup> are thermodynamically compatible with the (bio)electrocatalytic reduction of O<sub>2</sub> to water by Pt and a number of multi-copper enzymes, such as bilirubin oxidase (BOD), that can be directly wired to electrodes and are currently widely used for construction of enzymatic biofuel cells, as a green, cost-effective and sustainable alternative to precious metal catalysts<sup>23, 44-48</sup>.

hematite or TiO<sub>2</sub>) and an O<sub>2</sub>-reducing bilirubin oxidase/carbon cloth biocathode.

Performance of such a solar energy transforming device in such renewable medium as seawater is a challenging task, and if found feasible, opens new energetic and clean water production perspectives. Due to the high salt content, seawater represents a natural electrolyte solution for an electrochemical cell, and H<sub>2</sub>O/O<sub>2</sub> PEC cells operating in seawater will be free from any extra fuels and electrolyte, by directly converting solar energy into electrical power within the H<sub>2</sub>O-O<sub>2</sub>-H<sub>2</sub>O redox cycle. Along with that, large concentrations of chloride and some other anions present in seawater and its basic pH may have detrimental effects on both the photoanode and biocathode performance, to the extent that the redox cycling would be thermodynamically impossible. Hitherto, most of photoelectrocatalytic studies of semiconductor photoanodes were performed in a strong (1 M) alkaline medium<sup>39, 42, 49</sup>, and most of the O<sub>2</sub>-biocathode studies were performed in more acidic solutions<sup>23, 44, 45, 50, 51</sup>, with just a few examples of low-potential bacterial enzymes, operating directly in seawater<sup>52</sup>.

Here, we demonstrate that a hybrid bio-photovoltaic (BPV) cell is capable of recycling H<sub>2</sub>O/O<sub>2</sub> couple in environmental conditions-mimicking basic media and directly in seawater and produces electrical energy under sunlight illumination indeed (Figure 1). To our best knowledge, that is the first example of the hybrid semiconductor-enzymatic BPV cell operating in seawater, verifying the thermodynamic and kinetic feasibility of extracting energy from those environmental resources. It provides a sustainable and cost-effective solution to mitigating the energy and water crisis in the future, with such BPV cells applied for direct fresh water production at the biocathode.

## Results and discussion

The individual electrochemical performance of Zn-doped hematite and TiO<sub>2</sub> photoanodes and a BOD biocathode in seawater has been studied, prior to their coupling in the hybrid bio-photovoltaic cell, to establish the thermodynamic compatibility of the proposed system that would enable its operation as a galvanic element.

### Photoelectrocatalysis of water oxidation by Zn-doped hematite and TiO<sub>2</sub> photoanodes.

Photoactive Zn-doped and pristine hematite electrodes were produced by electrochemical deposition of iron oxides and Zn<sup>2+</sup> (when necessary) on the surface of the fluorine-doped tin oxide (FTO) electrodes, followed by the electrodes annealing at 800 °C, according to the previously reported procedure<sup>38</sup>. By this, stable red-brown nanostructured hematite films were formed on the FTO surface. They were extensively characterized in our previous work and in the current studies did not show any deviation from their previously reported morphological, chemical and electrochemical features<sup>42</sup>. The 1.9-2.2 eV hematite band-gap predetermines its ability to adsorb the visible-light photons with the wavelength below

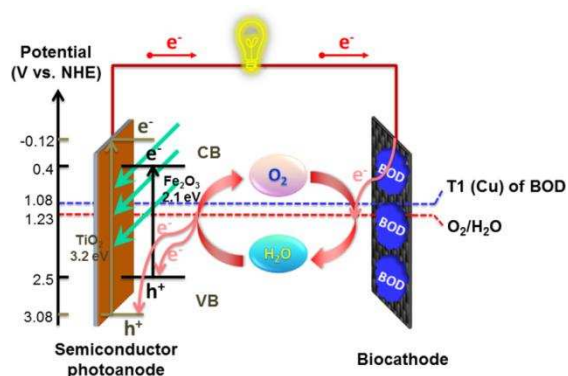


**Figure 1.** Schematic representation of the operation principle of a bio-photovoltaic cell consisting of a semiconductor photoanode (Zn-doped

600 nm, and its valence band edge position (2.5 eV) is positive enough to oxidize water (Figure 1). Compared to pristine hematite, Zn-doped hematite exhibits the enhanced photoelectrocatalytic activity, in 1 M NaOH lowering the overpotential of water oxidation by 218 mV (Figure S1, ESI), consistent with the accelerated kinetics of charge transfer between the surface states and water molecules and, as a result, of the water splitting reaction affected by Zn localized on the electrode surface<sup>38</sup>. Therewith, Zn-modified hematite surface has been shown to operate as a true water-oxidation catalyst decreasing the water oxidation potential.

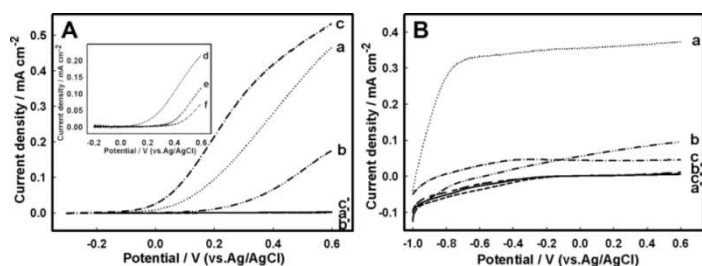


**Figure 2.** Representative linear sweep voltammograms (LSVs) of photoelectrocatalytic oxidation of water recorded with **(A)** Zn-doped hematite and **(B)** TiO<sub>2</sub> electrodes in (a, a') 1 M Tris-HCl and (b, b') seawater, both pH 8, and (c, c') 1 M NaOH, (a'-c') without and (a-c) under the light illumination (AM 1.5G, 100 mW cm<sup>-2</sup>). Potential scan rate: 5 mV s<sup>-1</sup>. Inset: Representative LSV of photoelectrocatalytic oxidation of water recorded with a Zn-doped hematite electrode in (d) 0.5 M Na<sub>2</sub>CO<sub>3</sub>-NaHCO<sub>3</sub>, pH 9.16, (e) 0.5 M Na<sub>2</sub>B<sub>4</sub>O<sub>7</sub>-H<sub>3</sub>BO<sub>3</sub>, pH 8, and (f) 0.5 M PBS, pH 8. Potential scan rate: 5 mV s<sup>-1</sup>.

As can be seen in Figure 2, in 1 M NaOH Zn-doped hematite shows the highest photoelectrocatalytic currents and the lowest onset potential for water oxidation, consistent with the previous reports<sup>38, 53</sup>. In 1 M Tris-HCl, pH 8, Zn-doped hematite still exhibits a sufficiently high photoelectrocatalytic activity and low potential for water oxidation, with a photocurrent density of 0.44 mA cm<sup>-2</sup> at 0.56 V (vs. Ag/AgCl, which is equivalent to 1.23 V vs. RHE) (Figure 2A). In the seawater medium, the photoelectrooxidation currents decrease 64%, to 0.16 mA cm<sup>-2</sup>, and the catalysis onset shifts from -100 mV (in Tris-HCl) to 70 mV (in seawater, pH 8), suggesting that photoelectrocatalysis in seawater is significantly inhibited by seawater components.

Such complex media as seawater may be approximated by the following ion content: [Cl<sup>-</sup>]: 559.40 mM, [Na<sup>+</sup>]: 480.57 mM, [K<sup>+</sup>]: 10.46 mM, [Mg<sup>2+</sup>]: 54.14 mM, [Ca<sup>2+</sup>]: 10.53 mM, [SO<sub>4</sub><sup>2-</sup>]: 28.93 mM, [HCO<sub>3</sub><sup>-</sup>]: 2.11 mM, [B(OH)<sub>3</sub>]: 0.43 mM, [PO<sub>4</sub><sup>3-</sup>]: 3.2 μM<sup>21, 54</sup>. Based on that composition, we evaluated the effect of Na<sup>+</sup>, Cl<sup>-</sup>, CO<sub>3</sub><sup>2-</sup>/HCO<sub>3</sub><sup>-</sup>, B<sub>4</sub>O<sub>7</sub><sup>2-</sup>, and HPO<sub>4</sub><sup>2-</sup>/H<sub>2</sub>PO<sub>4</sub><sup>-</sup> on the photoelectrocatalytic activity of Zn-doped hematite (Figure 2A). No distinct changes in the current or onset potential have been observed in buffer solutions with a high NaCl content. However, the nature of the anion of the buffer solution, such as carbonate, borate and phosphate anions, dramatically affected the photoelectrocatalytic performance of the photoanode (Figure 2A, inset).

The most pronounced (though reversible) depression of photoelectrocatalysis, reducing the photo-oxidation current densities to 0.05 mA cm<sup>-2</sup> at 0.56 V, was observed in the

phosphate buffer solutions, which very likely is connected with the formation of insoluble Zn phosphate deposits<sup>55</sup> on the surface of Zn-doped hematite, by this eliminating Zn from the reaction zone and fouling the photoanode surface. A strong inhibition of photoelectrocatalysis by phosphate anions excludes Zn-hematite-based BPV cells operation in phosphate-rich media, but not in seawater, where the phosphate content is quite low (3.2 μM). The inhibition of photoelectrocatalysis in carbonate solutions (2.11 mM in seawater) was quite similar to that observed in seawater, and for borate, which actual concentration in seawater is in a sub-mM range, it approached that characteristic of phosphate (Figure 2A, inset). In agreement with previous reports<sup>56</sup>, the Cl<sup>-</sup> anion itself did not contribute too much to the inhibition (see data for Tris-HCl), thus most of the inhibition of photoelectrocatalysis in seawater (compared to Tris-HCl of the same pH) may be associated with its borate and carbonate contents.

Photoelectrocatalytic oxidation of seawater was also studied at TiO<sub>2</sub> electrodes routinely used for photoelectrocatalytic water splitting<sup>57</sup>. In contrast to hematite, at the TiO<sub>2</sub> photoanodes photoelectrocatalysis of water oxidation started at much lower potentials, ca. -1.0 V, and the highest efficiency of bioelectrocatalyses was observed in Tris-HCl buffer solutions, with a limiting currents approaching 0.37 mA cm<sup>-2</sup> (Figure 2B). These currents are comparable with those at Zn-doped hematite observed at 0.6 V. Along with that, the onset of photoelectrocatalysis and the limiting current plateau occurred, as earlier mentioned, at much more negative potentials. The photoelectrocatalytic activity of the TiO<sub>2</sub> electrodes in seawater (and alkaline media) drops down to a larger extent than that of Zn-doped hematite, and the photocurrent at 0.56 V decreases by 75% (and 88%, respectively). Thus, despite the less favorable potential for photoelectrocatalytic water oxidation, Zn-doped hematite residual activity and stability in environmental media is higher, and its performance in such environment as seawater is somehow superior to TiO<sub>2</sub>.

Water oxidation on the TiO<sub>2</sub> surface<sup>58</sup> involves mechanistic routes different from those at hematite<sup>42, 59</sup>, including formation of several intermediates which redox transformation is strongly pH dependent, in particular, in basic solutions (pH 13) the formed surface Ti-O<sup>-</sup> species can be quickly oxidized by photogenerated holes, by this slowing down the water oxidation reaction<sup>60</sup>. The involvement of O<sub>2</sub> and and such products of its reduction (by the photoinduced e<sup>-</sup> in the conduction band) as superoxide anion radical O<sub>2</sub><sup>•-</sup>, and further routes of its transformation to H<sub>2</sub>O<sub>2</sub>, H<sub>2</sub>O and O<sub>2</sub>, cannot be excluded; all those steps depend both on pH<sup>61</sup> and solution composition<sup>62</sup> and thus can contribute to the energy losses in such complex matrix as seawater. Therewith, the Cl<sup>-</sup> anion itself does not inhibit photoelectrocatalysis (Figure 2B, data for 1 M Tris-HCl) and was even discussed to enhance the photoelectrocatalytic efficiency<sup>63</sup>.

### Bioelectrocatalytic reduction of O<sub>2</sub> at a bilirubin oxidase biocathode in basic media.

Quite a few enzymes can efficiently electrocatalyse oxygen reduction in basic solutions<sup>52, 64</sup>, and BOD is one of them<sup>65-67</sup>, currently being mostly used in glucose biofuel cells operating in physiological media<sup>47, 48</sup> and as a model enzyme in artificial photosynthesis cells, in which BOD oxidase cathodes are coupled to electrically wired photosystem-based photo-bioanodes<sup>23</sup>. As a member of a multicopper oxidoreductase family, BOD catalyses four electron reduction of oxygen to water at potentials approaching those at Pt in acidic media and is essentially stable both in neutral and slightly alkaline/Cl<sup>-</sup>-rich solutions<sup>46, 65, 68</sup>.

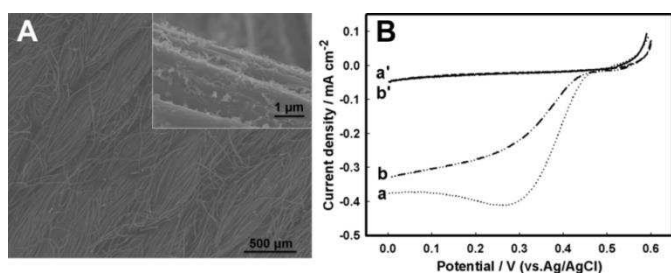


**Figure 3.** Representative (A) SEM images of GCC, inset: with enzyme cross-linked; and (B) LSVs recorded with the BOD/GCC electrode in (a', b') N<sub>2</sub>-saturated and (a, b) air-saturated (a', a) 1 M Tris-HCl, pH 8, and (b', b) seawater, pH 8. Scan rate is 5 mV s<sup>-1</sup>.

To design a simple, cost-effective, and still efficient BOD biocathode for O<sub>2</sub> reduction, we have immobilized and cross-linked BOD on the surface of the activated graphitized carbon-cloth (GCC) electrode<sup>69</sup>. GCC is an inexpensive and widely industrially used micro-fibrous textile material (Figure 3A) with outstanding flexibility and mechanical strength, which holds great promise as a high surface area, micro-structured substrate for enzyme immobilization and bioelectrocatalysis. However, GCC is inherently hydrophobic and to make it appropriate for enzyme immobilization; it was activated (hydrophilized) by oxidation in concentrated H<sub>2</sub>SO<sub>4</sub>, to generate more surface oxide functionalities<sup>70</sup>. Cross-linked on the GCC surface, BOD directly, with no mediators, bioelectrocatalytically reduced oxygen in air-saturated 1 M Tris-HCl, pH 8, starting from 0.5 V (Figure 3B), with O<sub>2</sub> diffusion-limited current densities that approached 0.4 mA cm<sup>-2</sup>. In seawater, the onset potential for bioelectrocatalysis slightly shifted to less positive potentials (0.49 V), and the efficiency of the reduction process 79% decreased compared to the original bioelectrocatalytic activity in 1 M Tris-HCl, with current densities reaching now 0.30 mA cm<sup>-2</sup>. Therewith, the Cl<sup>-</sup>-tolerance of BOD was much higher than that of fungal laccases, dropping down 30% in 0.15 M NaCl-containing pH 5 solutions<sup>69</sup> or 75% in seawater shown for low potential bacterial laccases such as SLAC<sup>52</sup>.

### Electrocatalysis of oxygen reduction at a Pt-mesh cathode.

Bioelectrocatalytic reduction of O<sub>2</sub> at the BOD/GCC biocathode was compared to that at a Pt mesh cathode, a

traditionally used electrocatalyst for O<sub>2</sub> reduction<sup>71, 72</sup>. The cleanliness of the electrode surface was verified in deaerated 0.5 M H<sub>2</sub>SO<sub>4</sub>, where the cyclic voltammograms (CVs) of a Pt mesh electrode exhibited typical features characteristic of a clean Pt surface, with three regions correlating with the adsorption/desorption of H atoms, the double-layer region and the region of Pt surface oxidation and reduction (Figure 4A). In 0.5 M H<sub>2</sub>SO<sub>4</sub> electrocatalysis of O<sub>2</sub> reduction at the Pt mesh surface started from 0.65 V and reached 0.16 mA cm<sup>-2</sup> at 0.43 V in a quiescent solution (Figure 4B).

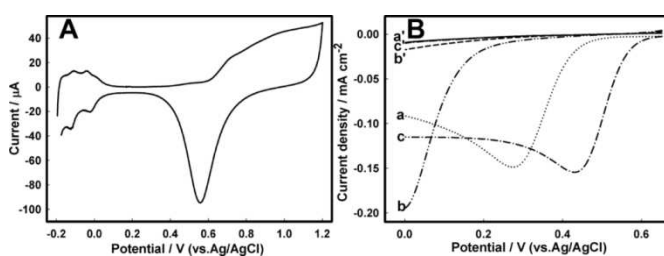


**Figure 4.** Representative (A) CV recorded with the Pt mesh electrode in 0.5 M H<sub>2</sub>SO<sub>4</sub> (scan rate: 25 mV s<sup>-1</sup>); and (B) LSVs recorded with the Pt mesh electrode in (a', b', c') N<sub>2</sub>-saturated and (a, b, c) air-saturated (a', a) 1 M Tris-HCl, pH 8, (b', b) seawater, pH 8, and (c', c) 0.5 M H<sub>2</sub>SO<sub>4</sub>, respectively. Scan rate: 5 mV s<sup>-1</sup>.

More basic pH significantly affected the electrocatalysis of the 4e<sup>-</sup>/2H<sup>+</sup>-coupled reduction of O<sub>2</sub> to H<sub>2</sub>O, mostly in its onset, shifting it to less positive values, though the efficiency of electrocatalysis in terms of current densities remained almost the same (0.15 mA cm<sup>-2</sup>, Figure 4B). However, in seawater a further almost 0.4 V shift of the half-wave potential to less positive values could be followed, very likely connected with the electrode fouling. Such performance apparently limits applications of Pt-based electrocatalysts in this media.

### Performance of the BPV cells.

Finally, the semiconductor photoanodes were coupled to the enzymatic BOD biocathode in a single membraneless biophotovoltaic cell, and efficiency of solar energy conversion to electricity was evaluated in terms of power densities produced by such BPV.

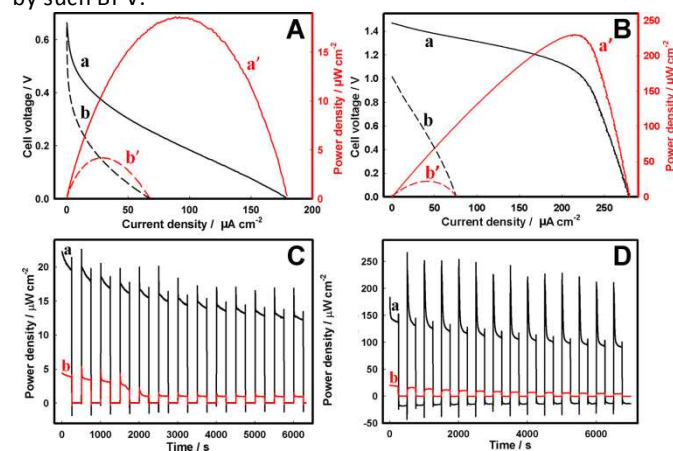


**Figure 5.** Representative dependencies of (a, b) the cell voltage and (a', b') cell power density on the cell current density recorded for the BPV cells

comprising (A) Zn-doped hematite and (B) TiO<sub>2</sub> photoanodes and the BOD/GCC biocathode. (C, D) Dependences of the power output of the BPV cells composed of (C) Zn-doped hematite and (D) TiO<sub>2</sub> photoanodes on cyclic on-off light switching; for (C): at (a) 0.2 V in 1 M Tris-HCl and (b) 0.16 V in seawater, both pH 8; for (D): at (a) 1.06 V in 1 M Tris-HCl and (b) 0.5 V in seawater. Light intensity: AM 1.5G, 100 mW cm<sup>-2</sup>; scan rate: 5 mV s<sup>-1</sup>.

The BPV cell comprising the Zn-doped hematite photoanode and the BOD/GCC biocathode gave the open-circuit voltage ( $V_{oc}$ ) of 0.66 V and 0.64 V in 1 M Tris-HCl and seawater, respectively (Figure 5, Table 1). The maximum power density ( $P_{max}$ ) produced by the cell in seawater was  $4.2 \pm 0.3 \mu\text{W cm}^{-2}$ , representing ca. 25% of the  $P_{max}$  in Tris-HCl ( $18.6 \pm 2.1 \mu\text{W cm}^{-2}$ ) (Figure 5A). Those results are consistent with the data in Figure 2A, demonstrating the essential drop of the photoanode activity in seawater (NB: but not that of the biocathode, Figure 3B), which performance becomes the limiting factor in the BPV operation. Even so, the power extracted from the Zn-doped hematite BPV cell is more than an order of magnitude higher than that generated by the photovoltaic cell comprising the Zn-doped hematite photoanode and Pt mesh cathode ( $0.32 \pm 0.01 \mu\text{W cm}^{-2}$ ), in which the performance of the Pt cathode is greatly inhibited by the electrode fouling in seawater (Figures 4B and 6). It also essentially exceeds  $0.87 \mu\text{W cm}^{-2}$  ( $8.7 \text{ mW m}^{-2}$ ) reported for a low temperature polymer electrolyte fuel cell driven by the water/proton concentration gradient between two electrodes electrochemically recycling the H<sub>2</sub>O/O<sub>2</sub> redox couple at 70 °C and pH 11<sup>73</sup>.

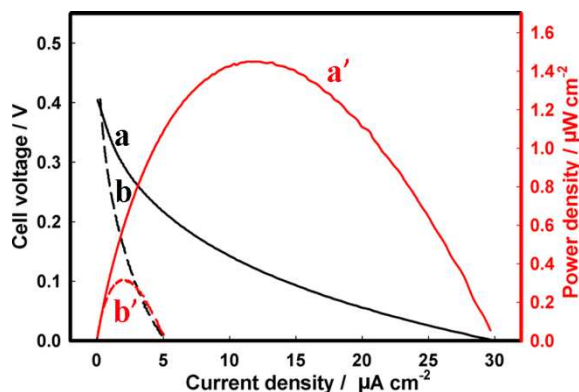


**Figure 6.** Representative (a, b) polarization and (a', b') power density – current density curves recorded for the photovoltaic cell comprising the Zn-doped hematite photoanode and the Pt mesh cathode in (a, a') 1 M Tris-HCl and (b, b') seawater, both pH 8.

As may be expected, the BPV cell comprising the TiO<sub>2</sub> photoanode and the BOD/GCC biocathode showed the  $V_{oc}$  and the  $P_{max}$  of 1.47 V and  $236 \mu\text{W} \pm 38 \text{ cm}^{-2}$  in 1 M Tris-HCl (Figure 5B) that actually approach the best results shown for direct ET-based enzymatic biofuel cells operating under conditions of O<sub>2</sub>-limited mass-transfer reactions<sup>43, 74, 75</sup> characteristic of environmental media. The cell fill factor  $FF$  of 0.57 was also quite high and approached that of dye-sensitized solar cells<sup>76</sup>, while for hematite cell it was only 0.16 (Table 1) consistent with a poorer performance of hematite, for which  $FF$  typically did not exceed 0.3<sup>77</sup>. In seawater (Figure 2B) the essential inhibition of photoelectrocatalytic currents of water oxidation

at the TiO<sub>2</sub> photoanodes resulted in the  $V_{oc}$  decreased to 1.01 V, and the  $P_{max}$  dropped sharply to less than 10% of its value in 1 M Tris-HCl (to  $21.4 \pm 4.1 \mu\text{W cm}^{-2}$ ) at 0.5 V. As in the case of the Zn-doped hematite BPV cell, such TiO<sub>2</sub> cell characteristics are consistent with the limiting performance of the photoanode, exhibiting the photoelectrocatalytic activity in seawater lower than the bioelectrocatalytic activity of the biocathode. The higher  $P_{max}$  generated from the TiO<sub>2</sub> BPV cell (Table 1) is mainly due to the higher cell voltage provided by the galvanic element formed by (H<sub>2</sub>O)TiO<sub>2</sub>/(O<sub>2</sub>)BOD rather than from the higher photocurrent values. Along with that, the higher tolerance of the Zn-doped hematite electrode towards operation in seawater implies the superior adaptability of Zn-doped hematite for operation in this environmental medium.

**Table 1.** Basic characteristics of the corresponding BVP cells (the  $V_{oc}$  and  $P_{max}$ ,<sup>a</sup> and fill factor  $FF$ ) in basic media studied

Design of the BPV cell	1 M Tris-HCl (pH 8.0)			Seawater (pH 8.0)		
	$V_{oc}$ (V)	$P_{max}$ ( $\mu\text{W cm}^{-2}$ )	$FF$	$V_{oc}$ (V)	$P_{max}$ ( $\mu\text{W cm}^{-2}$ )	$FF$
Photoanode-cathode type						
Zn-doped hematite - BOD/GCC	0.66±0.01	18.6±2.1 (at 0.20 V)	0.16	0.64±0.01	4.2±0.3 (at 0.16 V)	0.10
TiO <sub>2</sub> - BOD/GCC	1.47±0.02	236±38 (at 1.06 V)	0.57	1.01±0.01	21.4±4.1 (at 0.50 V)	0.28
Zn-doped hematite - Pt mesh	0.39±0.01	1.56±0.11 (at 0.19 V)	0.12	0.48±0.02	0.32±0.01 (at 0.15 V)	0.13

<sup>a</sup> without the sunlight illumination (dark cell conditions) the  $P_{max}$  did not exceed  $44 \text{ nW cm}^{-2}$  for Zn-hematite systems (ESI, Figures S2-S5), TiO<sub>2</sub> systems did not properly work as a galvanic element in the dark.

Finally, the operational stability of the BPV cells in basic media was evaluated by the on-off cyclic illumination of the photoanodes, and the variation of the  $P_{max}$  with time, in response to the repeated light stimulation, was recorded (Figure 5C,D). Both Zn-doped hematite and TiO<sub>2</sub> BPV cells exhibited fast photo-responses to constantly switching dark and light operations. With time, though, the power generated by both BPV cells slightly decreased, in seawater quite quickly, in 40 min for Zn-doped hematite and in 60 min for TiO<sub>2</sub> reaching a steady-state level, suggesting that it can be continuously used as a sustainable electrical energy supply. Among two studied systems, the Zn-doped hematite BPV cell was found to be most stable, with a minimal activity loss upon repeated use, currently demonstrating preferential stability features important for continuous energy transformations in the sea medium.

## Conclusions and Perspectives

Here, we have demonstrated a clean, sustainable and low-cost production of electricity from readily available environmental resources such as sea water, O<sub>2</sub> and sunlight, by coupling in a single galvanic element sunlight-illuminated semiconductor

photoanodes, able to photoelectrocatalytically oxidize  $\text{H}_2\text{O}$ , and  $\text{O}_2$ -reducing enzymatic biocathodes.  $\text{H}_2\text{O}/\text{O}_2$  recycling in such system does not need additional fuel, but only sunlight and seawater and thus is *totally sustainable*. This technology<sup>78</sup> represents a new concept for sustainable generation of electricity from environmental media and represents an advanced and simpler alternative to the existing solar biofuel

cells exploiting biological photosystems wired to electrodes and coupled either to laccase or BOD-oxygen biocathodes (Table 2). The showed proof-of-concept operation of such bio-photovoltaic cells currently producing  $236 \mu\text{W cm}^{-2}$  in 1 M Tris-HCl and  $21.4 \mu\text{W cm}^{-2}$  in seawater, both pH 8, is comparable to the existing enzymatic biofuel cells operating under direct ET-conditions in air-saturated solutions<sup>43, 52, 74, 75</sup>.

**Table 2.** Basic electrochemical characteristics of the hitherto developed membrane-less direct ET-based solar biofuel cells operating under air-saturating conditions (FF was calculated where it was possible).

Cell design	Operational conditions	$V_{oc}$ , V	$J_{sc}$ , $\mu\text{A cm}^{-2}$	P, $\mu\text{W cm}^{-2}$	FF	Ref.
TiO <sub>2</sub> NPs/FTO vs. BOD/carbon cloth cathode	Photoelectrocatalytic oxidation of $\text{H}_2\text{O}$ and bioelectrocatalytic reduction of $\text{O}_2$ , 1 M Tris, pH 8, 100 $\text{mW cm}^{-2}$ illumination	1.47 V	280 $\mu\text{A cm}^{-2}$	236 $\mu\text{W cm}^{-2}$ at 1.06 V	0.57	this work
Chlorine- $e_g$ /TiO <sub>2</sub> vs. bilirubin oxidase/ABTS cathode	Photooxidation of NADH for enzymatic oxidation of glucose, 10 mM Tris, pH 7, 100 $\text{mW}/\text{cm}^2$	0.53 V	9 $\mu\text{A cm}^{-2}$	1.7 $\mu\text{W cm}^{-2}$ at 0.4 V	0.36	<sup>79</sup>
Cyanobacteria/carbon nanotubes (CNT) vs. laccase/carbon paper cathode	Bioelectrocatalytic oxidation of $\text{H}_2\text{O}$ and reduction of $\text{O}_2$ , 0.1 M phosphate, pH 5.8, 76 $\text{mW cm}^{-2}$ illumination.	0.57,	24 $\mu\text{A cm}^{-2}$ ;	3.5 $\mu\text{W cm}^{-2}$ at 0.33 V	0.26;	<sup>80</sup>
Thylacoid membranes/ multiwall carbon nanotubes vs. laccase/ MWCNT cathode	Bioelectrocatalytic oxidation of water and reduction of $\text{O}_2$ , 0.1 M phosphate, pH 6.8, 80 $\text{mW cm}^{-2}$ illumination.	0.35 V	68 $\mu\text{A cm}^{-2}$	5.3 $\mu\text{W cm}^{-2}$ at 0.2 V	0.22	<sup>25</sup>
Thylacoid membranes/ Toray paper vs. Nafion/laccase/anthracene-modified MWCNT	Bioelectrocatalytic oxidation of $\text{H}_2\text{O}$ and reduction of $\text{O}_2$ , citrate buffer pH 5.5, light: 250 W halogen lamp at 5200 lumens	0.72 V	14 $\mu\text{A cm}^{-2}$	$\sim 1.8 \mu\text{W cm}^{-2}$ at 0.3 V	0.17	<sup>24</sup>
TiO <sub>2</sub> nanotubes vs. BOD/carbon nanotube cathode	Photoelectrocatalytic oxidation of glucose – reduction of $\text{O}_2$ , 0.1 M phosphate, pH 7, 50 $\text{mW cm}^{-2}$ UV light illumination	1 V	Not reported	47 $\mu\text{W cm}^{-2}$ at 0.79 V	-	<sup>30</sup>
Poly(mercapto- <i>p</i> -benzoquinone)/ photosystem II/Au vs. BOD/CNT cathode	Bioelectrocatalytic oxidation of water and reduction of $\text{O}_2$ , 0.1 M phosphate, pH 7.4, 0.10 W at wavelength > 400 nm	0.43 V	114 $\mu\text{A cm}^{-2}$	17 $\mu\text{W cm}^{-2}$ at 0.28 V	0.35	<sup>23</sup>
ITO/SnO <sub>2</sub> NPs/ tetraaryl-phorphyrin sensitizer vs. Hg/HgSO <sub>4</sub> cathode	Photo-oxidation of NADH for enzymatic photo-oxidation of glucose, 0.25 M Tris, pH 8, 1 $\text{mW cm}^{-2}$ at 520 nm	0.75 V	60 $\mu\text{A}$	18 $\mu\text{W cm}^{-2}$ t 0.42 V	0.42	<sup>81</sup>

In those hybrid bio-photovoltaic devices, the solar-light-excited electrons flow up in the conduction band of the semiconductor photoanode and then in the external circuit, and the holes in the valence band of the semiconductor allow oxidation of water to molecular oxygen and protons. The electrons transferred through the external circuit to the biocathode allow re-reduction  $\text{O}_2$  diffusing from the photoanode to biocathode into water (or reduction of environmentally supplied  $\text{O}_2$ ). The net reaction is the solar energy conversion to electricity in the ceaseless cycle of water consumption and regeneration with no necessity of a membrane between two electrodes lowering the internal resistance of the setup and improving the energy utilization efficiency (Figure 1).

The current state-of-the-art data show that the cell performance can be improved to  $3 \text{ mW cm}^{-2}$  once open circuit cell voltages > 1 V and current densities >  $10 \text{ mA cm}^{-2}$  in neutral solutions will be achieved<sup>63, 82</sup>. Then, it may become comparable with the existing technologies (in average  $\sim 10 \text{ mW cm}^{-2}$  for silicon solar cells), along with that, offering a ca. 5 fold decrease in  $\text{W cm}^{-2}$  costs at the expense of cheaper and more sustainable materials used (estimations based on all material costs except of FTO). Attributed to the low expenditure and simple preparation, such type of BPV cells can be expected to

find their practical industrial applications and potentially contribute to lessening of the energy crisis.

Another possible application of such BPV cells is a self-powered fresh water production at biocathodes that can be directly correlated with the electricity costs. The lack of sufficient safe water supplies to satisfy human needs in many regions of the Earth, also in well-developed such as California, positions clean water production among the main global challenges for humanity<sup>83</sup>. In future perspectives, these BPV systems may contribute not only to the electricity production, but also to the direct fresh water production at the biocathodes or be used indirectly, to power seawater desalination systems<sup>84</sup>.

However, the current performance of the BPV cells in seawater is strongly limited by the photoanode operation. While existing biotechnologies allow the development of up 1 year stabilized biocathodes<sup>85</sup>, exhibiting  $5\text{--}10 \text{ mA cm}^{-2}$  steady-state current densities and  $>8 \text{ mW cm}^{-2}$  power output in advanced enzymatic biofuel cell designs (air-breathing gas-diffusion biocathodes)<sup>86, 87</sup>, which performance in seawater is not expected to be essentially different (Figure 3B), performance of the photoanodes in seawater requires focusing of the research efforts.

Two problems should be solved, both contributing to the development of the “ideal” photoanode. Those are stabilization of the existing semiconductor systems against inhibition in seawater and further lowering of the potential for water oxidation. While a strong research is conducted to enhance the photoelectrocatalytic performance of photoanodes in such media as NaOH, with the reported impressive photocurrent densities between 2 and 5 mA cm<sup>-2</sup>, at 1.23 V versus RHE, for example at silicon-doped  $\alpha$ -Fe<sub>2</sub>O<sub>3</sub> electrodes<sup>34</sup> or Pt-doped single-crystalline hematite electrodes<sup>88</sup>, their operation in less conventional but more abundant media is not straightforward. It is also a matter of the efficiency achieved versus the cost and sustainability of the materials used. The cheapest materials so far are iron, titanium and zinc oxides, plentifully available from naturally existing minerals – and the way they can be modified by similarly inexpensive and sustainable metal dopants or surface protective layers/islets of relevant catalytic activity<sup>89</sup>, to allow clean production of energy on a massive scale. For example, the efficient electrocatalytic and photoelectrocatalytic oxidation of water can be achieved at graphite and hematite electrodes modified with trace amounts of Ir oxide nanoparticles<sup>38, 90</sup>, however, even in the case of trace amounts, the relation between the cost and efficiency can be still the limiting application factor.

## Experimental

### Materials.

Fluorine-doped tin oxide coated glass (FTO, TEC-15) was from Nippon Sheet Glass, Japan. Ferric chloride (FeCl<sub>3</sub>·6H<sub>2</sub>O), potassium chloride, zinc(II) chloride, potassium fluoride, and 30% hydrogen peroxide of A. R. grade were from Sigma-Aldrich. Titanium (IV) oxide powder (TiO<sub>2</sub>, P25, according to the producer, mixed rutile and anatase phase, average nanoparticle size of 21±5 nm) was from Degussa AG, Germany. The graphitized carbon cloth (GCC) with an apportioned surface of ca. 10 m<sup>2</sup> g<sup>-1</sup> and specific resistance of 0.04  $\Omega$  cm was from Electrougli NIPT of Carbon Wares (Russian Federation). The surface roughness of GCC was of 10-30 and the pyrographite overweight was about 10%<sup>43</sup>. Tris(hydroxymethyl)aminomethane chloride (Tris-HCl), hydrochloric acid, BS<sup>3</sup> (the cross-linker), and bilirubin oxidase from *Myrothecium verrucaria* (BOD) with the activity of 15-65 U mg<sup>-1</sup> of protein were from Sigma-Aldrich. All aqueous solutions were prepared with Milli-Q Ultrapure Water (Millipore Corp, 18.25 M $\Omega$  cm<sup>-1</sup> at 25 °C). Seawater was collected from the sea area in Aarhus, Denmark, and filtered before use (final pH 8.0).

### Preparation of Zn-doped hematite and TiO<sub>2</sub> photoanodes.

Electrochemical deposition of Zn-doped hematite on FTO electrodes was carried out according to the previously reported protocol<sup>38</sup> with a little modification. Before electrodeposition, the FTO electrodes were ultrasonically cleaned in several 10 min steps, in pure water, ethanol,

acetone, and finally rinsed in water again. The electrodeposition solution contained 5 mM FeCl<sub>3</sub>, 0.025 mM ZnCl<sub>2</sub>, 5 mM KF, 0.1 M KCl dissolved in water and 1 M H<sub>2</sub>O<sub>2</sub>. *In situ* electrodeposition of nanostructured Zn-doped hematite on clean FTO electrodes was carried out by cyclic voltammetry in a three-electrode cell at 50 °C, by cycling the potential between -0.48 V and 0.42 V (100 cycles) with a scan rate of 0.2 V s<sup>-1</sup>. After the electrodeposition step, the modified electrodes were thoroughly rinsed with water, dried at rt and annealed in the preheated oven at 800 °C for 10 min in the air, the original yellowish film on the electrode surface transforming into the red one. Those electrodes are referred to as the Zn-doped hematite photoanodes<sup>38</sup>. TiO<sub>2</sub> electrodes were prepared by blading P25 TiO<sub>2</sub> nanoparticle dispersion (4 mg mL<sup>-1</sup> in ethanol) onto FTO electrode and dried at rt. The electrodes were fitted in a homemade Teflon holder exposing 0.3 cm<sup>2</sup> of the photoanode geometrical area to the solar simulator lamp irradiation (1.5 AM, 150 W, LS0108, LOT-QuantumDesign GmbH, Germany). The incident light intensity of the solar simulator was 100 mW cm<sup>-2</sup> as calibrated with a reference silicon solar cell (RR-234, Rera Solutions, B. V., The Netherlands) before the photoelectrochemical experiments.

### Preparation of BOD/GCC biocathode.

Before modification, GCC (2 cm × 1 cm pieces) was, first, soaked in 10 M sulfuric acid for 2 hours to oxidatively remove all contaminants and hydrophilise otherwise the hydrophobic surface of GCC<sup>43</sup>. Then, the GCC was rinsed carefully with excess of water and left overnight in water. The enzyme immobilization was performed by following a slightly modified procedure reported in<sup>23</sup>. More specifically, 1 mg of BOD was dissolved in 1 mL of a 0.1 M HEPES buffer solution, pH 8, and 30  $\mu$ L of this solution was spread onto the GCC electrode. After 30 min immobilization at 4 °C, the BOD immobilized on the GCC electrode was cross-linked by adding 10  $\mu$ L of 1 mg mL<sup>-1</sup> of aqueous solution of BS<sup>3</sup> (reacting for another 1.5 h). The resulting biocathode is referred to as a BOD/GCC electrode. The electrode surface area was restricted to 0.3 cm<sup>2</sup> by an insulating adhesive tape. The morphology of the electrodes was characterized by a field-emission scanning electron microscope (Nova NanoSEM 600, FEI, USA) at an accelerating voltage of 15 kV.

### Pretreatment of the Pt mesh electrode.

Before the electrochemical measurements, the Pt mesh electrode (1.6×1.0 cm<sup>2</sup>) was successively cleaned chemically in 1 M HCl and acetone, and electrochemically in 0.5 M H<sub>2</sub>SO<sub>4</sub>. The electrochemically active surface area of the polycrystalline Pt electrode determined from the peak of the surface oxides reduction in CVs recorded in 0.5 M H<sub>2</sub>SO<sub>4</sub> using the normalization coefficient of 420  $\mu$ C cm<sup>-2</sup><sup>91</sup> was 0.3 cm<sup>2</sup>, close to the surface area of the anode used.

### BPV cell assemblies and measurements.

The BPV cell was assembled by combining the Teflon holder-sealed photoanode and the BOD/GCC biocathode, with a distance between them of 0.5 cm. The simulated solar light

lamp (1.5 AM, 100 mW cm<sup>-2</sup>) was placed right over the air-exhibited surface of the semiconductor photoanode in such a way that the light beam approach the surface perpendicularly. The BPV cell operation was tested in 30 mL 1M Tris-HCl buffer solution, pH 8, and seawater, pH 8. In control experiments, the BOD/GCC biocathode was replaced by the Pt mesh electrode.

#### Electrochemical measurements.

All electrochemical measurements were carried out with a  $\mu$ Autolab potentiostat (Metrohm Autolab B.V. Metrohm AG, The Netherlands) equipped with a Nova 1.8 software. In the three-electrode configuration, an Ag/AgCl (saturated KCl) electrode was the reference electrode and a Pt flag electrode was the counter electrode. In the two electrode configuration, a semiconductor photoanode and a biocathode (alternatively, a Pt mesh cathode) were used. The fill factor (FF) of the cell was calculated using the equation 1:

$$FF = \frac{P_{max}}{V_{oc} J_{sc}} \quad (1)$$

where  $J_{sc}$  is the short-circuit current density,  $V_{oc}$  the open-circuit voltage,  $P_{max}$  is the maximum power density generated by BPV cell and  $P_{in}$  is power density of the input light.

#### References

1. N. Armaroli and V. Balzani, *Angew. Chem. Int. Ed.*, 2007, **46**, 52-66.
2. J. Potočník, *Science*, 2007, **315**, 810.
3. U. S. Department of Energy, *Basic research needs for solar energy utilization* 2005.
4. N. S. Lewis and D. G. Nocera, *Proc. Nat. Acad. Sci. USA*, 2006, **103**, 15729-15735.
5. S. H. Lee, J. H. Kim and C. B. Park, *Chem. Eur. J.*, 2013, **19**, 4392-4406.
6. M. Grätzel, *Nature*, 2001, **414**, 338-344.
7. X. Y. Chen, S. Shen, L. Guo and S. S. Mao, *Chem. Rev.*, 2010, **110**, 6503-6570.
8. K. Sivula and R. van de Krol, *Nature Rev.*, 2016, **1**, 1-15.
9. W. Shockley and H. J. Queisser, *J. Appl. Phys.*, 1961, **32**, 510-519.
10. T. Saga, *NPG Asia Mater*, 2010, **2**, 96-102.
11. D. Yu, M. Yin, L. Lu, H. Zhang, X. Chen, X. Zhu, J. Che and D. Li, *Adv. Mater.*, 2015, **27**, 6747-6752.
12. D. J. Norris and E. S. Aydil, *Science*, 2012, **338**, 625-626.
13. M. M. Lee, J. Teuscher, T. Miyasaka, T. N. Murakami and H. J. Snaith, *Science*, 2012, **338**, 643-647.
14. in <https://www.linkedin.com/pulse/2-million-tons-solar-scrap-every-year-2030-whose-m-v-radhakrishna>, <https://www.linkedin.com/pulse/2-million-tons-solar-scrap-every-year-2030-whose-m-v-radhakrishna>.
15. M. Grätzel, R. A. Janssen, D. B. Mitzi and E. H. Sargent, *Nature*, 2012, **488**, 304.
16. Y.-J. Hwang, H. Li, B. A. E. Courtright, S. Subramaniam and S. A. Jenekhe, *Adv. Mater.*, 2016, **28**, 124-131.
17. H. Bente, T. Nishida, D. Mori, H. Xu, H. Ohkita and S. Ito, *Energ. Environ. Sci.*, 2016, **9**, 135-140.
18. W. Nie, H. Tsai, R. Asadpour, J.-C. Blancon, A. J. Neukirch, G. Gupta, J. J. Crochet, M. Chhowalla, S. Tretiak, M. A. Alam, H.-L. Wang and A. D. Mohite, *Science*, 2015, **347**, 522-525.
19. H. J. Snaith, *J. Phys. Chem. Lett.*, 2013, **4**, 3623-3630.
20. M. Grätzel, *Acc. Chem. Res.*, 2009, **42**, 1788-1798.
21. <http://gcell.com/dye-sensitized-solar-cells>, 2016
22. S. Tsujimura, A. Wadano, K. Kano and T. Ikeda, *Enz. Microb. Technol.*, 2001, **29**, 225-231.
23. O. Yehezkeli, R. Tel-Vered, J. Wasserman, A. Trifonov, D. Michaeli, R. Nechushtai and I. Willner, *Nat. Commun.*, 2012, **3**, 742.
24. M. Rasmussen, A. Shrier and S. D. Minteer, *Phys. Chem. Chem. Phys.*, 2013, **15**, 9062-9065.
25. J. O. Calkins, Y. Umasankar, H. O'Neill and R. P. Ramasamy, *Energ. Environ. Sci.*, 2013, **6**, 1891-1900.
26. Q. Gui, Z. Xu, H. Zhang, C. Cheng, X. Zhu, M. Yin, Y. Song, L. Lu, X. Chen and D. Li, *ACS Appl. Mater. Interfaces*, 2014, **6**, 17053-17058.
27. A. Fujishima and K. Honda, *Nature*, 1972, **238**, 37-38.
28. M. Miyauchi, A. Nakajima, T. Watanabe and K. Hashimoto, *Chem. Mater.*, 2002, **14**, 2812-2816.
29. Q. Chen, J. Li, X. Li, K. Huang, B. Zhou, W. Cai and W. Shangguan, *Environ. Sci. Technol.*, 2012, **46**, 11451-11458.
30. L. Han, L. Bai, C. Zhu, Y. Wang and S. Dong, *Chem. Commun.*, 2012, **48**, 6103-6105.
31. A. Duret and M. Grätzel, *J. Phys. Chem. B*, 2005, **109**, 17184-17191.
32. L. Xia, J. Bai, J. Li, Q. Zeng, X. Li and B. Zhou, *Appl. Catal. B: Environ.*, 2016, **183**, 224-230.
33. S. Chen, S. S. Thind and A. Chen, *Electrochem. Comm.*, 2016, **63**, 10-17.
34. A. Kay, I. Cesar and M. Grätzel, *J. Am. Chem. Soc.*, 2006, **128**.
35. P. Dias, A. Vilanova, T. Lopes, L. Andrade and A. Mendes, *Nano Energy*, 2016, **23**, 70-79.
36. S. C. Warren, K. Voitchovsky, H. Dotan, C. M. Leroy, M. Cornuc, F. Stellacci, C. Hebert, A. Rothschild and M. Grätzel, *Nature Mater.*, 2013, **12**, 842-849.
37. S. C. Riha, B. M. Klahr, E. C. Tyo, S. Seifert, S. Vajda, M. J. Pellin, T. W. Hamann and A. B. F. Martinson, *ACS Nano*, 2013, **3**, 2396-2405.
38. N. Mirbagheri, J. Chevallier, J. Kibsgaard, F. Besenbacher and E. E. Ferapontova, *ChemPhysChem*, 2014, **15**, 2844-2850.
39. Y. Zhang, S. Jiang, W. Song, P. Zhou, H. Ji, W. Ma, W. Hao, C. Chen and J. Zhao, *Energ Environ. Sci.*, 2015, **8**, 1231-1236.
40. X. Liu, Y. Yang, L. G. Mao, Z. J. Li, C. J. Zhou, X. H. Liu, S. Zheng and Y. X. Hu, *Sens. Actuat. B*, 2015, **218**.
41. S. do Amaral Carminati, F. L. Souza and A. F. Nogueira, *ChemPhysChem*, 2016, **17**, 170-177.
42. N. Mirbagheri, D. Wang, C. Peng, J. Wang, Q. Huang, C. Fan and E. E. Ferapontova, *ACS Catalysis*, 2014, **4**, 2006-2015.
43. U. B. Jensen, S. Lörcher, M. Vagin, J. Chevallier, S. Shipovskov, O. Koroleva, F. Besenbacher and E. E. Ferapontova, *Electrochim. Acta*, 2012, **62**, 218-226.
44. K. Murata, K. Kajiya, N. Nakamura and H. Ohno, *Energ Environ. Sci.*, 2009, **2**, 1280-1285.
45. R. J. Lopez, S. Babanova, Y. Ulyanova, S. Singhal and P. Atanassov, *ChemElectroChem*, 2014, **1**, 241-248.
46. N. Mano and L. Edembe, *Biosens. Bioelectron.*, 2013, **50**, 478-485.
47. N. Mano, F. Mao and A. Heller, *J. Am. Chem. Soc.*, 2003, **125**, 6588-6594.
48. M. Cadet, S. Gounel, C. Stines-Chaumeil, X. Brilland, J. Rouhana, F. Louerat and N. Mano, *Biosens. Bioelectron.*, 2016, **83**, 60-67.
49. S. Hoang, S. Guo, N. T. Hahn, A. J. Bard and C. B. Mullins, *Nano Letters*, 2012, **12**, 26-32.
50. S. C. Barton, H.-H. Kim, G. Binyamin, Y. Zhang and A. Heller, *J. Am. Chem. Soc.*, 2001, **123**, 5802-5803.

51. C. F. Blanford, C. E. Foster, R. S. Heath and F. A. Armstrong, *Faraday Discuss.*, 2008, **140**, 319-335.
52. S. Lörcher, P. Lopes, A. Kartashov and E. E. Ferapontova, *ChemPhysChem* 2013, **14**, 2112
53. C. J. Sartoretti, B. D. Alexander, R. Solarska, W. A. Rutkowska, J. Augustynski and R. Cerny, *J. Phys. Chem. B*, 2005, **109**, 13685-13692.
54. M. E. Q. Pilson, *An Introduction to the Chemistry of the Sea*, Prentice Hall, 1998.
55. W. Shin, J. Lee, Y. Kim, H. Steinfink and A. Heller, *J. Am. Chem. Soc.*, 2005, **127**, 14590-14591.
56. K. Shimizu, A. Lasia and J.-F. Boily, *Langmuir*, 2012, **28**, 7914-7920.
57. K. Lee, A. Mazare and P. Schmuki, *Chem. Rev.*, 2014, **114**, 9385-9454.
58. T. Berger, D. Monllor-Satoca, M. Jankulovska, T. Lana-Villarreal and R. Gómez, *ChemPhysChem*, 2012, **13**, 2824-2875.
59. K. G. U. Wijayantha, S. Saremi-Yarahmadi and L. M. Peter, *Phys. Chem. Chem. Phys.*, 2011, **13**, 5264-5270.
60. A. Imanishi, T. Okamura, N. Ohashi, R. Nakamura and Y. Nakato, *J. Am. Chem. Soc.*, 2007, **129**, 11569-11578.
61. S. Shipovskov, E. E. Ferapontova, I. Gazaryan and T. Ruzgas, *Bioelectrochem.*, 2004, **63**, 277-280.
62. S.-Y. Lee and S.-J. Park, *J. Industr. Eng. Chem.*, 2013, **19**, 1761-1769.
63. X. Zang, H. Cui, M. Humayun, Y. Qu, N. Fan, X. Sun and L. Jing, *Sci. Reports*, 2016, **6**, 21430.
64. I. R. Wheeldon, J. W. Gallaway, S. C. Barton and S. Banta, *Proc. Natl. Acad. Sci. USA*, 2008, **105**, 15275-15280.
65. N. Mano, H.-H. Kim and A. Heller, *J. Phys. Chem. B.*, 2002, **106**, 8842-8848.
66. N. Mano, J. L. Fernandez, Y. Kim, W. Shin, A. J. Bard and A. Heller, *J. Am. Chem. Soc.*, 2003, **125**, 15290-15291.
67. L. dos Santos, V. Climent, C. F. Blanford and F. A. Armstrong, *PhysChemChemPhys.*, 2010, **12**, 13962-13974
68. F. Durand, C. H. Kjaergaard, E. Suraniti, S. Gounel, R. G. Hadt, E. I. Solomon and N. Mano, *Biosens. Bioelectron.*, 2012, **35**, 140-146.
69. U. B. Jensen, M. Vagin, O. Koroleva, D. S. Sutherland, F. Besenbacher and E. E. Ferapontova, *J. Electroanal. Chem.*, 2012, **667** 11-18.
70. A. A. Karyakin, M. Y. Vagin, S. Z. Ozkan and G. P. Karpachova, *J. Phys. Chem. B*, 2004, **108**, 11591-11595.
71. S. Mukerjee, S. Srinivasan, M. P. Soriaga and J. McBreen, *J. Electrochem. Soc.*, 1995, **142**, 1409-1422.
72. J. Wu and H. Yang, *Acc. Chem. Res.*, 2013, **46**, 1848-1857.
73. A. M. Dreizler and E. Roduner, *Energy Environ. Sci.*, 2010, **3**, 761-764.
74. E. Nazaruk, M. Karaskiewicz, K. Żelechowska, J. F. Biernat, J. Rogalski and R. Bilewicz, *Electrochem. Comm.*, 2012, **14**, 67-70.
75. Y. Kamitaka, S. Tsujimura, N. Setoyama, T. Kajino and K. Kano, *Phys. Chem. Chem. Phys.*, 2007, **9**, 1793-1801.
76. J. Cong, Y. Hao, L. Sun and L. Kloo, *Adv. Energy mater.*, 2014, **4**, paper 1301273.
77. B. M. Klahr and T. W. Hamann, *Appl. Phys. Lett.*, 2011, **99**, article 063508.
78. *Denmark Pat.*, 2016.
79. Y. Amao, Y. Sakai and Y. Teshima, *Res. Chem. Intermed*, 2016, **42**, 7761-7770.
80. N. Sekar, Y. Umasankar and R. P. Ramasamy, *Phys. Chem. Chem. Phys.*, 2014, **16**, 7862-7871.
81. L. de la Garza, G. Jeong, P. A. Liddell, T. Sotomura, T. A. Moore, A. L. Moore and D. Gust, *J. Phys. Chem. B*, 2003, **107**, 10252-10260.
82. P. Y. Kuang, Y. Z. Su, K. Xiao, Z. Q. Liu, N. Li, H. J. Wang and J. Zhang, *ACS Appl. Mat. Inter.*, 2015, **7**, 16387-16394.
83. <http://www.millennium-project.org/millennium/challeng.html>, 2016
84. K. N. Knust, D. Hlushkou, U. Tallarek and R. M. Crooks, *ChemElectroChem*, 2014, **1**, 850-857.
85. M. J. Moehlenbrock and S. D. Minteer, *Chem. Soc. Rev.*, 2008, **37**, 1188-1196.
86. K. So, S. Kawai, Y. Hamano, Y. Kitazumi, O. Shirai, M. Hibi, J. Ogawa and K. Kano, *Phys. Chem. Chem. Phys.*, 2014, **16**, 4823-4829.
87. K. So, Y. Kitazumi, O. Shirai, S. Kawai, K. Nishikawa, Y. Higuchi and K. Kano, *J. Mater. Chem. A*, 2016, **4**, 8712-8719.
88. J. Y. Kim, G. Magesh, D. H. Youn, J.-W. Jang, J. Kubota, K. Domen and J. S. Lee, *Sci. Reports*, 2013, **3**, 2681.
89. J. O. M. Bockris and A. K. N. Reedy, *Modern Electrochemistry*, Kluwer Academic Publishers, New York, 2004.
90. S. D. Tilley, M. Cornuz, K. Sivula and M. Grätzel, *Angew. Chem. Int. Ed.*, 2010, **49**, 6405-6408.
91. S. Trasatti and O. A. Petrii, *Pure Appl. Chem.*, 1991, **63**, 711-734.